Carbohydrate Polymers 114 (2014) 213–221

Contents lists available at ScienceDirect

Carbohydrate Polymers

journal homepage: www.elsevier.com/locate/carbpol

Three-dimensional electrospun polycaprolactone (PCL)/alginate hybrid composite scaffolds

Min Seong Kim, GeunHyung Kim*

Department of Biomechatronic Engineering, College of Biotechnology and Bioengineering, Sungkyunkwan University (SKKU), Suwon, 440-746, Republic of Korea

ARTICLE INFO

Article history:
Received 27 January 2014
Received in revised form 15 July 2014
Accepted 1 August 2014
Available online 19 August 2014

Keywords:
Alginate
Polycaprolactone
Composite
3D scaffold
Tissue engineering

ABSTRACT

Micro/nanofibrous scaffolds have been used widely in biomedical applications because the micro/nano-scale fibres resemble natural extracellular matrix and the high surface-to-volume ratio encourages cellular activities (attachment and proliferation). However, poor mechanical properties, low controllability of various shapes and difficulties in obtaining controllable pore structure have been obstacles to their use in hard-tissue regeneration. To overcome these shortcomings, we suggest a new composite system, which uses a combination method of wet electrospinning, rapid prototyping and a physical punching process. Using the process, we obtained polycaprolactone (PCL)/alginate composite scaffolds, consisting of electrospun PCL/alginate fibres and micro-sized PCL struts, with mean pore sizes of 821 ± 55 μm. To show the feasibility of the scaffolds for hard-tissue regeneration, the scaffolds were assessed not only for physical properties, including hydrophilicity, water absorption, and tensile and compressive strength, but also *in vitro* cellular responses (cell viability and proliferation) and osteogenic differentiation (alkaline phosphatase (ALP) activity, and mineralisation) by culturing with pre-osteoblasts (MC3T3-E1 cells). With the reinforcing micro-sized PCL struts, the elastic modulus of the PCL/alginate scaffold was significantly improved versus a pure PCL scaffold. Additionally, due to the alginate component in the fibrous scaffold, they showed significantly enhanced hydrophilic behaviour, water absorption (~8-fold) and significant biological activities (~1.6-fold for cell viability at 7 days, ~2.3-fold for ALP activity at 14 days and ~6.4-fold for calcium mineralisation at 14 days) compared with those of a pure PCL fibrous scaffold.

1. Introduction

Tissue engineering has been introduced as a promising method of repairing large defect areas in bone tissue. To achieve successful regeneration of bone, biomedical scaffolds are required because they perform pivotal roles in seeding osteoblasts and guiding new bone formation into the desired shapes (Hutmacher & Biomater, 2001Langer et al., 1995; Ma, 2004; Vacanti & Langer, 1999; Yang, Leong, Du, & Chua, 2001).

To successfully regenerate bone tissue, an engineered scaffold needs a physically stable and structurally porous shape, having high pore interconnectivity, high porosity and appropriate surface topography. Appropriate pore size and 100% pore interconnectivity not only provide for the migration and proliferation of osteoblasts, but also enable the efficient diffusion of various growth factors and rapid vascularisation (Murphy, Haugh, & O'Brien, 2010).

To regenerate hard tissues, various synthetic polymers, such as poly(glycolic acid) (PGA), poly(lactic acid) (PLA), poly(lactic-co-glycolic acid) (PLGA) and poly(ε-caprolactone) (PCL), have been investigated as biomedical scaffold materials. Of them, PCL is a biocompatible and biodegradable aliphatic polyester and has appropriate mechanical strength and good processability in many shapes, so it has been considered as a potential biomaterial for bone tissue regeneration (Kneser, Rath, Pryymachuk, & Bleiziffer, 2011Petrie Aronin et al., 2008). However, like other synthetic polymers, it is hydrophobic in nature, impeding the penetration of aqueous cell suspensions into the interior structure and has poor cell recognition sites, leading to poor cell affinity and adhesion (Melchels et al., 2010). Additionally, PCL can produce acidic by-products during degradation, causing an inflammatory response (Wu, Wan, Dalai, & Zhang 2010). To overcome these deficiencies, PCL may be blended and/or composited with other synthetic or natural polymers (Koenig & Huang, 1995; Kweon et al., 2003; Zhu, Gao, Liu, & Shen, 2002).

Generally, natural biopolymers (e.g. hyaluronic acid, alginate, collagen, chitosan, elastin) show enzyme-controlled degradability,

* Corresponding author. Tel.: +82 31 290 7828.
E-mail address: gkimbme@skku.edu (G. Kim).

http://dx.doi.org/10.1016/j.carbpol.2014.08.008
0144-8617/

good biocompatibility, low inflammatory potential, high chemical versatility and similarities with the extracellular matrix (Malafaya, Silva, & Reis, 2007). Generally, alginates have been a popular polysaccharide for tissue engineering applications. Alginates consist of α-L-guluronic acid (G) and β-D-mannuronic acid (M) units, and have easy gelation properties with outstanding biocompatibility, biodegradability, low immunological stimulation and easy controllability into a designed shape (Cohen, Malone, Lipson, & Bonassar, 2006). However, unfortunately, this natural polymer has poor mechanical properties and limited 3D shape-ability due to its hydrophilic nature, so that chemical or physical alterations and blend/composite systems are commonly used to enhance its low mechanical strength and low processability.

Several methods of preparing biomedical scaffolds based on micro/nano-fabrication have been developed (Gallego, Ferrell, Sun, & Hansford, 2008; Hollister, 2005; Kapyla et al., 2012). Of them, electrospinning is an easy and effective method for fabrication of micro/nanofibrous tissue-engineered scaffolds (Barnes, Sell, Boland, Simpson, & Bowlin, 2007; Liang, Hsiao, & Chu, 2007; Ma, Kotaki, Inai, & Ramakrishna, 2005; Pham, Sharma, & Mikos, 2006).

Electrospun fibres have great potential in that the structure, particularly that of micro/nano-scale fibres, resembles the natural extracellular matrix (ECM) and shows a high surface-to-volume ratio, which promotes cellular activities such as attachment and proliferation (Li, Laurencin, Caterson, Tuan, & Ko, 2002). However, although this method has several advantages, it also has some drawbacks that may prevent its use in various tissue regenerative materials. These include small pore size, low controllability of 3D structure and poor mechanical properties. Small pore size and low 3D shape-ability of the fibrous structure constrain the infiltration and migration of seeded cells and regeneration of large and complex tissues. Additionally, the poor mechanical properties are a major limitation to its use in hard-tissue regeneration. To overcome these shortcomings, various methods including modification of fibre diameter (Soliman et al., 2011), post-processing by photo-patterning (Galperin, Long, & Ratner, 2010), 3D-structured nanofibre layers using several patterned collectors (Vaquette & Cooper-White, 2011), wet-electrospun 3D fibrous mats (Kim et al., 2014) and a stacked direct-write electrospinning nanofibrous mat (Lee, Jang, Oh, Jeong, & Cho, 2013), have been suggested.

In this study, we introduce a new method of fabricating highly porous PCL-based 3D micro/nanofibrous scaffolds with improved mechanical properties and a controllable, homogeneous pore size. To overcome the shortcomings of PCL as a scaffold material, we accommodated alginate with a dispersed phase in the fibrous scaffold. Additionally, to improve the mechanical properties, rapid-prototyped PCL struts were embedded in the fibrous structure. The scaffold was finally post-processed with a physical punching method to obtain sufficient pores (~820 μm) channelling from the top to the bottom of the scaffold. The final fabricated scaffold showed high porosity (~92%) and outstanding mechanical properties. Furthermore, the biological performance of the scaffold was evaluated using pre-osteoblasts (MC3T3-E1) to determine whether the dispersed alginate component in the composite scaffold affected various cellular activities *in vitro*, as assessed using the MTT assay, fluorescence imaging and evaluation of alkaline phosphatase (ALP) activity and calcium mineralisation.

2. Experimental

2.1. Materials

Low-viscosity and high G-content LF10/60 alginate (FMC BioPolymer, Drammen, Norway) and crosslinking agent, $CaCl_2$ (Sigma–Aldrich), of the alginate were used. Poly(ε-caprolactone) (PCL) (density = 1.135 g/cm^3, melting temperature = 60 °C, M_n = 60,000 g/mol) was purchased from Sigma–Aldrich (USA).

2.2. Fabrication of 3D fibrous scaffolds

To obtain micro-sized struts of PCL, PCL powder was injected into a heating cylinder at 130 °C, and the melted PCL was extruded through a heated 250-μm nozzle. The perpendicular struts were plotted with a three-axis robot system. The speed of the plotter nozzle was set at 5 mm/s, and the applied pneumatic pressure was set at 550 ± 20 kPa. Additionally, to prepare PCL/alginate micro/nanofibres, various weight fractions (1, 3, 5 wt%) of alginate and PCL (10 wt%) in a 20:80 solvent mixture of methylene chloride (MC, Junsei Chem. Co.) and dimethyl formamide (DMF, Junsei Chem. Co.) were used with a 21-G electrospinning nozzle and a 20-mL glass syringe. In the target chamber, 95% ethyl alcohol (EtOH, Duksan, Korea) was supplied. The surface tension and density of EtOH are 0.0223 N/m and 0.808 g/cm^3, respectively. An applied electric field (1 ± 0.2 kV/cm) and a fixed flow rate of 0.5 mL/h were used. As a target, an EtOH bath was used, and the supply rate (10 mL/min) of EtOH was controlled using a flow meter with a grounded copper plate immersed in the bath. Details of the fabrication of the bath were described previously (Kim et al., 2014). After fabricating the PCL/alginate scaffolds, they were immersed in 10 wt% $CaCl_2$ for 10 min. After this cross-linking process, they were washed with PBS. To obtain dried 3D fibrous structures, the structures were vacuum freeze dried using a freeze dryer (SFDSM06; Samwon, Busan, South Korea) at −76 °C for 2 days. The flow rate of the PCL/alginate solution was controlled using a syringe pump (KDS 230; KD Scientific, Holliston, MA, USA). A power supply (SHV300RD-50 K; Convertech, Seoul, South Korea) was used to produce the electric field. We designated the pure PCL fibrous scaffold, and PCL/alginate-5 wt% fibrous scaffolds with and without the layer of micro-sized PCL struts as "PP", "PA-S", and "PA", respectively.

2.3. Characterisation of the fibrous scaffolds

A scanning electron microscope (SEM, SNE-3000 M, SEC Inc., South Korea) was used to characterise the surface morphology of the fibrous scaffolds. Cell morphology was also evaluated by SEM.

To measure the hydrophilic properties of the scaffolds, one droplet (10 μL) of water mixed with red dye was carefully dropped onto the surface of the scaffolds, and the hydrophilic behaviour was captured with a digital camera over various time periods. Water absorption was calculated by weighing the samples before and after soaking in distilled water for 12 h. The percentage increase in water absorption was calculated as $(\%) = (W_{12\,h} - W_o)/W_o \times 100$, where $W_{12\,h}$ was the weight of the sample after 12 h, and W_o was the original weight of the sample.

To assess the mechanical properties, we used two testing methods, tensile and compression. To measure mechanical properties, the scaffolds were cut into small strip shapes ($8 \times 10\,mm^2$ for the tensile test) and cylindrical shapes (diameter = 8 mm and thickness = 3.3 ± 2 mm for the compression test). Tests were conducted using a tensile instrument (Top-tech 2000; Chemilab, Kyunggi-Do, South Korea). The tensile test was performed in a 'dry' state. The stress-strain curves were recorded at a stretching and compression speed of 0.5 mm/s. All values are expressed as means ± standard deviation (n = 4).

A Fourier-transform infrared (FT-IR) spectrometer (model 6700; Nicolet, West Point, PA, USA) was used to compare the chemical structures of PCL, alginate, and the PCL/alginate mixture. IR spectra represent the mean of 30 scans at 500–4000 cm^{-1} at a resolution of 8 cm^{-1}.

2.4. In vitro cell culture

Samples ($6 \times 6\ mm^2$) were sterilised with 70% ethanol and ultraviolet (UV) light, and then placed in culture medium overnight. Mouse pre-osteoblast cells (MC3T3-E1) of passage five in scaffolds were cultured in 24-well plates in α-minimum essential medium (Life Sciences, USA) containing 10% foetal bovine serum (Gemini Bio-Products, USA) and 1% antibiotic (Antimycotic, Cellgro, USA). The cells were seeded onto scaffolds at a density of 1×10^5 per sample, and incubated at 37 °C in an atmosphere of 5% CO_2. The medium was changed every second day.

2.5. MTT assay

Cell viability was determined using the MTT assay (Cell Proliferation Kit I, Boehringer Mannheim, Mannheim, Germany). This assay is based on cleavage of the yellow tetrazolium salt MTT by mitochondrial dehydrogenases in viable cells to produce purple formazan crystals. Cells on the scaffold were incubated with 0.5 mg/mL MTT for 4 h at 37 °C, and the absorbance at 570 nm was measured using a microplate reader (EL800; Bio-Tek Instruments, Winooski, VT). Five samples were tested for each incubation period, and each test was performed in triplicate.

2.6. Fluorescence images

After 1, 3 and 7 days in cell culture, the scaffolds were exposed to 0.15 mM calcein AM and 2 mM ethidium homodimer-1 for 45 min in an incubator to permit observation of live and dead cells. The stained specimens were visualised under a microscope (TE2000-S; Nikon, Tokyo, Japan) equipped with an epifluorescence attachment and a SPOT RT digital camera (SPOT Imaging Solutions, Sterling Heights, MI). Stained images were captured; green and red indicated live and dead cells, respectively. After 7 and 14 days of cell culture, the scaffolds were subjected to diamidino-2-phenylindole (DAPI) fluorescence staining to detect cell nuclei. Phalloidin (Invitrogen, Carlsbad, CA) staining was also performed to visualise the actin cytoskeleton of proliferated cells. The same fluorescence microscope was used to obtain the images.

2.7. ALP activity

ALP was assayed by measuring the release of *p*-nitrophenol (pNP) from *p*-nitrophenyl phosphate (pNPP). The scaffolds seeded with MC3T3-E1 were rinsed gently with phosphate buffered saline (PBS) and incubated for 10 min in Tris buffer (10 mM, pH 7.5) containing 0.1% Triton X-100 surfactant. Then, the lysate (100 μL) was added to the wells of 96-well plates containing 100 μL of pNPP solution, prepared using an ALP kit (procedure no. ALP-10; Sigma–Aldrich). In the presence of ALP, pNPP is converted to pNP and inorganic phosphate. ALP activity was determined from the absorbance at 405 nm using a microplate reader (Spectra III; SLT Lab Instruments, Salzburg, Austria). The value (unit) of ALP activity was normalised relative to the total protein content (mg).

2.8. Alizarin red S staining

Calcium mineralisation was determined by alizarin red S staining of MC3T3-E1 cells in 24-well plates. The cells were cultured in α-MEM containing 50 μg/mL vitamin C and 10 mM β-glycerophosphate. The cells were then washed three times with PBS, fixed in 70% (v/v) cold ethanol (4 °C) for 1 h and air-dried. The ethanol-fixed specimens were stained with 40 mM alizarin red S (pH 4.2) for 1 h and washed three times with purified water. The specimens were then destained with 10% cetylpyridium chloride in 10 mM sodium–phosphate buffer (pH 7.0) for 15 min. An optical microscope was used to observe the staining. The optical density (OD) of mineralisation was normalised relative to the total protein content.

2.9. Total protein content

The total protein content was measured using the bicinchoninic acid (BCA) protein assay (Pierce Kit; Thermo Scientific). Cell/scaffold samples were assayed after culturing for 7 and 14 days. Specimens were washed with PBS and lysed with 1 mL of 0.1% Triton X-100. An aliquot of the lysate (25 μL) was added to 200 μL of BCA working reagent, and the mixture was incubated for 30 min at 37 °C. The absorbance at 562 nm was determined using a plate reader.

2.10. Statistical analyses

All data are presented as means ± standard deviation. Statistical analyses were performed using the SPSS software (ver. 20.0; SPSS, Inc., Chicago, IL), and included single-factor analyses of variance (ANOVA). In all analyses, P values < 0.05 were considered to indicate statistical significance. “NS” indicates no statistically significant difference.

3. Results and discussion

3.1. Fabrication of PCL/alginate composite scaffold

The porous structure of biomedical scaffolds in bone tissue regeneration is an important design criterion because the pore structure (pore size, porosity and 100% pore interconnectivity) affects neovascularisation and even the effective exchange of nutrients and metabolic waste within the scaffold (Karageorgiou & Kaplan, 2005). In this work, PCL/alginate fibrous scaffolds were fabricated using a combined method with wet electrospinning and a rapid-prototype process. First, using a melt-plotting machine, melted PCL was plotted with a perpendicular mesh structure on a working stage (Fig. 1(a)). The cylindrical strut diameter was 305 ± 17 μm and the pore size, defined as the distance between the struts, was 1500 μm. Second, electrospun PCL/alginate fibres were deposited on the layer consisting of PCL struts in an EtOH bath, as shown in Fig. 1(b). In this process, ethanol was used as a medium to obtain the 3D fibrous structure of PCL/alginate, because the electrospun PCL/alginate fibres settled slowly in the ethanol bath, indicating that control of the ethanol (surface tension = 0.023 N/m) supply rate can be used to manipulate the thickness of the final fibrous construction, while the electrospun fibres do not subside in pure water due to its relatively high surface tension (0.073 N/m). More details of the mechanism of wet electrospinning were described in our previous report (Hong & Kim, 2011). As shown in the schematic in Fig. 1(c), this process was repeated three times, so that the rapid-prototyped micro-size-PCL struts were fully embedded in the PCL/alginate nanofibrous structure. Third, the fabricated PCL/alginate composite was post-processed to obtain relatively large pores (~820 μm; Fig. 1(d)). Specifically, to obtain a uniform pore size, the scaffold was frozen at −76 °C to sustain the 3D structure during the process; it was then punched through with a sharp steel rod (diameter = 800 μm), as shown in Fig. 1(d). Previously, we had attempted to obtain large pores (~500 μm) using a femto-second laser process. However, slightly melted fibres were seen on the surface of pores due to the laser (Rezwan, Chen, Blaker, & Boccaccini, 2006). Finally, a highly porous PCL/alginate scaffold with embedded PCL struts was obtained (Fig. 1(e)).

Fig. 2(a–d) show SEM images of pure PCL fibres and PCL/alginate fibres fabricated with various alginate weight fractions (1, 3 and 5 wt%), respectively. The average diameters of pure PCL

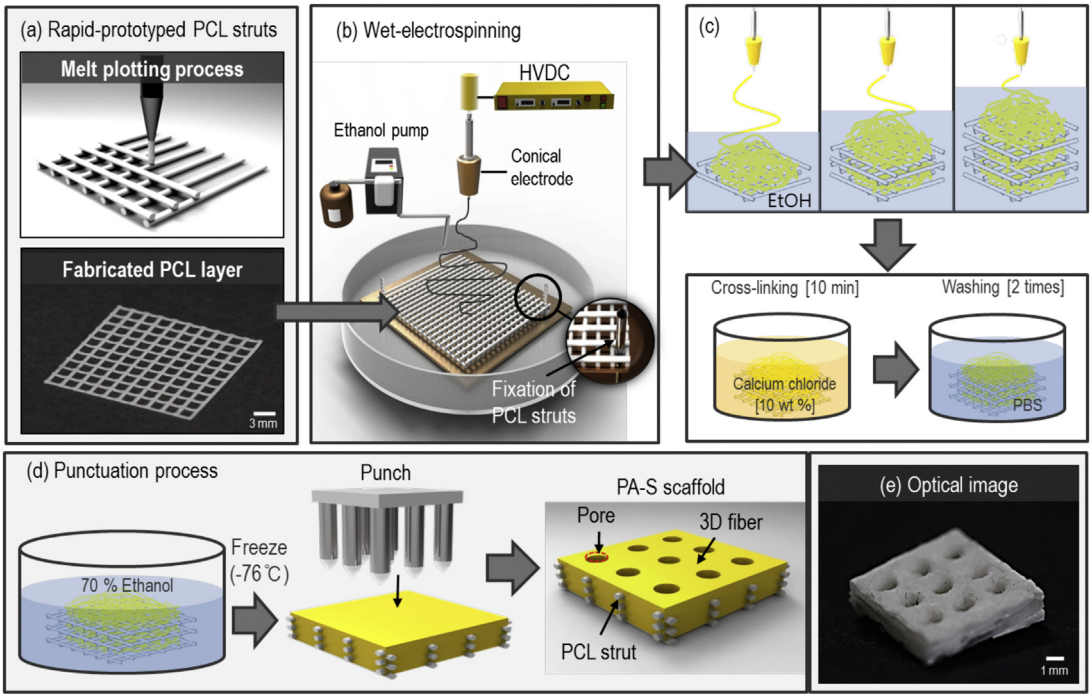

Fig. 1. Schematic of fabrication of a PCL/alginate fibrous scaffold with inserted PCL micro-struts. (a) Rapid-prototyping process for fabrication of micro-sized PCL struts, (b) wet-electrospinning process, (c) layer-by-layer structure consisting of PCL/alginate fibres and layers of perpendicular PCL struts, (d) punching process to produce micro-sized pores, and (e) an optical image of the final PCL/alginate (PA-S) scaffold with layered PCL struts.

fibres, PCL/alginate-1 wt%, PCL/alginate-3 wt% and PCL/alginate-5 wt% were 2.16 ± 0.33, 2.51 ± 0.31, 2.14 ± 0.41 and 1.67 ± 0.37 μm, respectively. The different fibre diameters resulted from the differing viscosity, conductivity and surface tension of the PCL/alginate solutions. The PCL solution had a conductivity of 2.52 μs/cm and surface tension of 0.018 (N/m), while for PCL/alginate-5 wt%, the conductivity and surface tension were 1.30 μs/cm and 0.016 (N/m), respectively. Additionally, as seen in the images, the alginate component in the mixture was not fully developed into a fibrous shape. However, because our goal was to achieve a homogeneous dispersion of alginate in the structure, the fabricated morphological structures are reasonable. Detailed conductivity and surface tension data for all samples are provided in Table 1.

Fig. 2(e) shows FT-IR spectra of pure alginate, PCL and PCL/alginate-5 wt% fibres. The spectrum of pure PCL contains a strong peak at 1722 cm^{-1} attributing to C=O stretching. In the pure alginate spectra, carboxyl peak near 1602 cm^{-1} characterises symmetric COO^- stretching vibrations, and asymmetric COO^- stretching vibrations were presented at 1417 cm^{-1}. The FTIR spectra of PCL/alginate indicate that the alginate was well dispersed within the PCL fibrous structure.

Generally, to increase the bioactive properties of the synthetic polymers, dispersed bioactive materials should be embedded as much as possible, if this does not reduce other physical properties significantly. Thus, we sought to fabricate electrospun PCL/alginate fibres using over 5 wt% of alginate in the mixture, but the electrospinnability was too low because of the high weight of the alginate component in the mixture.

Based on the processing conditions, we attempted to fabricate PCL/alginate fibrous scaffolds with and without embedded PCL struts, using a rapid-prototyping method. In this work, we assessed three 3D scaffolds: a pure PCL fibrous scaffold (PP, control), PCL/alginate-5 wt% fibrous scaffold (PA), and PCL/alginate-5 wt% fibrous scaffold with embedded perpendicular PCL struts (PA-S).

Fig. 2(f–h) show optical and SEM images of the final scaffolds (PP, PA and PA-S). The pores (mean pore size = 820.9 ± 46.9 μm, 823.5 ± 71.1 μm, and 819.1 ± 49.5 μm, respectively) were fabricated homogeneously using the punching process, from surface to bottom. The surface and cross-sectional SEM images demonstrate that the 3D scaffolds consisted of the electrospun fibres, the fibres of which in the inner pore surface were sustained; no melting was evident. In our previous work, fibres in the inner pore surface, generated by a femto-laser process, showed slight melting (Kim et al., 2014). Additionally, as shown in the cross-sectional SEM image of the PA-S scaffold, the micro-sized PCL struts were well embedded in the scaffold. Details of the pore structure, pore size, and porosity are provided in Table 2.

3.2. Hydrophilic properties and water absorption

The hydrophilic properties of a scaffold for bone tissue regeneration are important for induction of early cell attachment and growth because osteoblasts favour hydrophilic surfaces (Rezwan et al., 2006; Zhou, Hutmacher, Varawan, & Lim, 2007). To evaluate the hydrophilic properties of the scaffolds, a water droplet (10 μL) was mixed with red dye, and dropped on to the surface of the scaffolds (PP, PA, PA-S). Because alginate is hydrophilic in nature, we would expect the PCL/alginate composite to exhibit much stronger hydrophilic properties than pure PCL. This can be evaluated using the images in Fig. 3(a–c). As shown in the side and surface-view images, the water droplet was not absorbed in the pure PCL in 10 min, while the PCL/alginate scaffolds showed outstanding absorption almost instantaneously. The water absorption behaviour of the PA and PA-S scaffolds was similar.

Sufficient water absorption is an essential prerequisite for numerous scaffolds, because this can affect the absorption of body fluids and the transport of nutrients and metabolites within the scaffolds, eventually resulting in cell proliferation and the morphology of the regenerated tissue (Hollister, 2005; Roosa, Kemppainen,

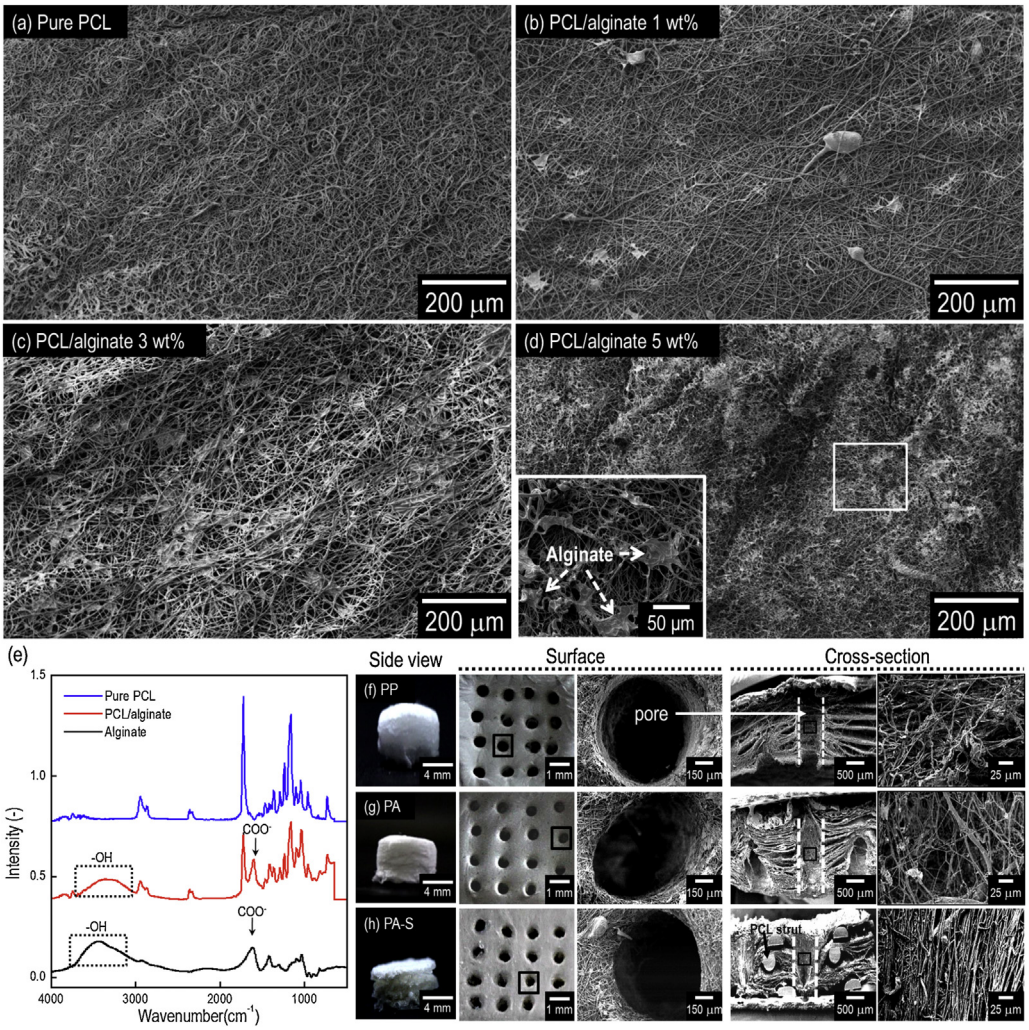

Fig. 2. SEM images of electrospun (a) pure PCL and PCL/alginate micro/nanofibres with various weight fractions of alginate ((b) 1 wt%, (c) 3 wt%, (d) 5 wt%). (e) FT-IR result for pure PCL, alginate and PCL/alginate-5 wt%. Surface and cross-sectional optical and SEM images of (f) PP (pure PCL), (g) PA (PCL/alginate-5 wt% without micro-sized PCL struts), and (h) PA-S (PCL/alginate-5 wt% with micro-sized PCL struts) scaffolds.

Table 1
Conductivity and surface tension of mixtures of PCL and various weight fractions (1, 3, 5 wt%) of alginate.

Sample type	Pure PCL	PCL/alginate 1 wt%	PCL/alginate 3 wt%	PCL/alginate 5 wt%
Conductivity (μs/cm)	2.52	1.56	1.42	1.30
Surface tension(N/m)	0.018	0.013	0.014	0.016

Moffitt, Krebsbach, & Hollister, 2010). Fig. 3(d) shows water absorption by the PP, PA and PA-S scaffolds. As expected, the addition of alginate to the scaffold (PA) resulted in greater water absorption than the pure PCL scaffold (PP). The PA-S scaffold with embedded PCL struts showed lower absorption compared with the PA scaffold. This was likely because of the embedded PCL struts, which occupy some volume within the PA-S scaffold. However, although the water absorption of the PA-S was low relative to the PA scaffold, water absorption by the PA-S was ~4-fold greater than that of the pure PCL scaffold.

The water absorption results for the PA scaffolds indicated that the alginate component in the PCL fibrous structure was well distributed and a small weight percentage (5 wt%) of alginate is sufficient to increase the hydrophilic properties of PA scaffolds. Based on these results, it would be expected that the PA scaffolds will show considerable cellular activities, initial cell attachment and proliferation *in vitro*, due to the accessibility of sustaining nutrients.

3.3. Mechanical properties

The mechanical properties of scaffolds are also important in sustaining physical shape during the regeneration of neo-tissues; they also affect various cellular activities, proliferation and the cytoskeleton (Discher, Janmey, & Wang, 2005). Fig. 4(a) shows Young's modulus: the modulus of the PP was 0.22 ± 0.04 MPa, that of PA was 0.23 ± 0.02 MPa, and that of PA-S was 4.3 ± 0.6 MPa. The maximum tensile strengths of PP, PA and PA-S were 322 ± 5, 54 ± 7, and 729 ± 41 kPa, respectively. Unlike the Young's modulus, the

Table 2
Pore structures (pore size and porosity) of the PP, PA and PA-S scaffolds.

Sample type	PP	PA	PA-S
Pore size (μm)	820.89 ± 46.97	823.49 ± 71.05	819.09 ± 49.46
Porosity (%)	98.05	97.38	91.86

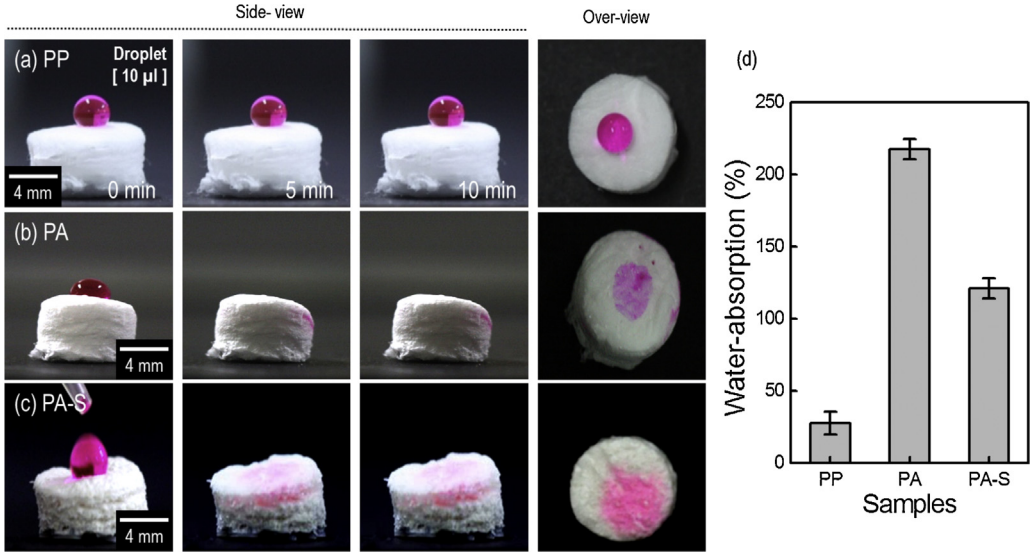

Fig. 3. Hydrophilic properties of (a) PP, (b) PA and (c) PA-S scaffolds for various time periods. (d) Water absorption by scaffolds.

difference in maximum strength between PP and PA was significant. The maximum strength of the PA scaffold was reduced significantly by addition of the alginate component, relative to PP, because when the external stress was fully applied to the entire PA scaffold, it was concentrated in the alginate component, which has a significantly lower Young's modulus, 9.2% that of pure PCL. However, for the PA-S scaffold, the modulus and maximum strength were markedly enhanced, ~20-fold and 2.3-fold, relative to the pure PCL scaffold due to the reinforcing micro-sized PCL struts.

Fig. 4(b) shows the compressive moduli of the PP, PA and PA-S scaffolds. As expected, the PA-S scaffold showed a higher compressive modulus (116.7 ± 10.6 kPa) compared with the PP (3.6 ± 0.3 kPa) and PA (30.5 ± 5.3 kPa) scaffolds. Also, the PA scaffold showed a meaningfully higher compressive modulus than the PP scaffold, because the alginate component plays a reinforcing role to endure the compressive stress.

To observe the effect of an embedded PCL layer consisted of microsized cylindrical struts on the tensile property, we measured the tensile property of PCL/alginate-5 wt% scaffolds, which have three different geometries of PCL layers (strut diameter = 305 ± 17 μm and pore size = 300, 1000 and 1500 μm). In the PCL layers (Fig. 1(a)), the pore size was defined as a distance between the cylindrical PCL struts. Fig. 4(c) show the Young's modulus and maximum strength. As shown in the results, the mechanical properties of the scaffolds were dependent significantly on the geometry of the embedded PCL layers. Based on the results, we can conclude that the mechanical properties of the scaffolds can be easily manipulated with the embedded layers of the PCL struts.

3.4. In vitro cellular activities

Pre-osteoblast (MC3T3-E1) cells were cultured on the fibrous scaffolds to evaluate cellular activity (cell viability and proliferation). Cell viability is one of the most important factors for evaluating biomedical scaffolds because it directly influences the final cellular activities, such as proliferation and differentiation. To observe cell viability on the fibrous scaffolds, pre-osteoblast cells were stained with calcein AM and ethidium homodimer-1 to enumerate live and dead cells. Fig. 5(a–c) show fluorescence images of live (green) and dead (red) cells on the PP, PA and PA-S scaffolds after culture for 1 or 7 days. At day 1, although the dispersed phase, alginate, cannot induce high cell-adhesion due to lack of cell-binding sites, cell attachment to the PA and PA-S fibrous scaffolds was considerably greater than on the pure PCL fibrous scaffold (PP), due to the enhanced hydrophilic properties and good wetting behaviour of PA and PA-S. This tendency of the scaffolds was similar after 7 days of culture.

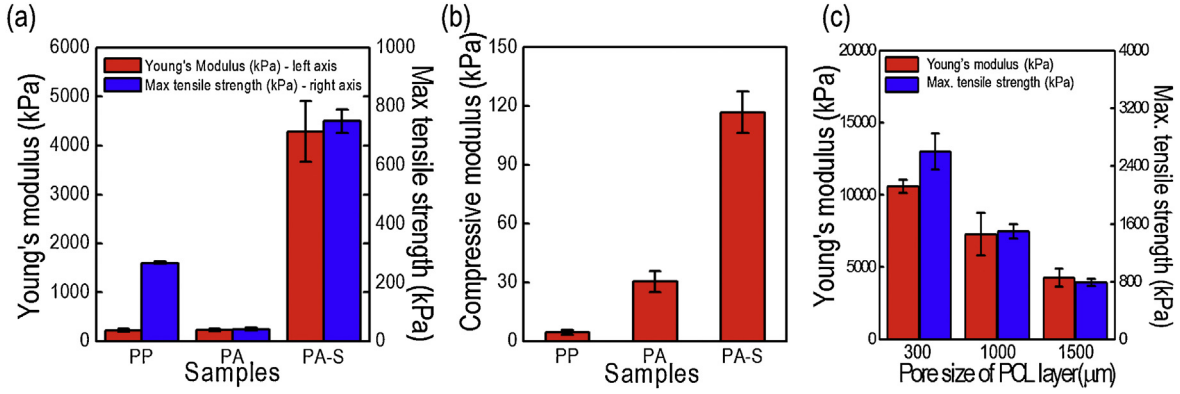

Fig. 4. Mechanical properties of PP, PA and PA-S scaffolds. (a) Young's and (b) compressive moduli in a tensile and compression test. (c) Young's modulus and maximum tensile strength for the PCL/alginate-5 wt% scaffolds having various pore sizes (300, 1000 and 1500 μm) of the interlayered PCL structure.

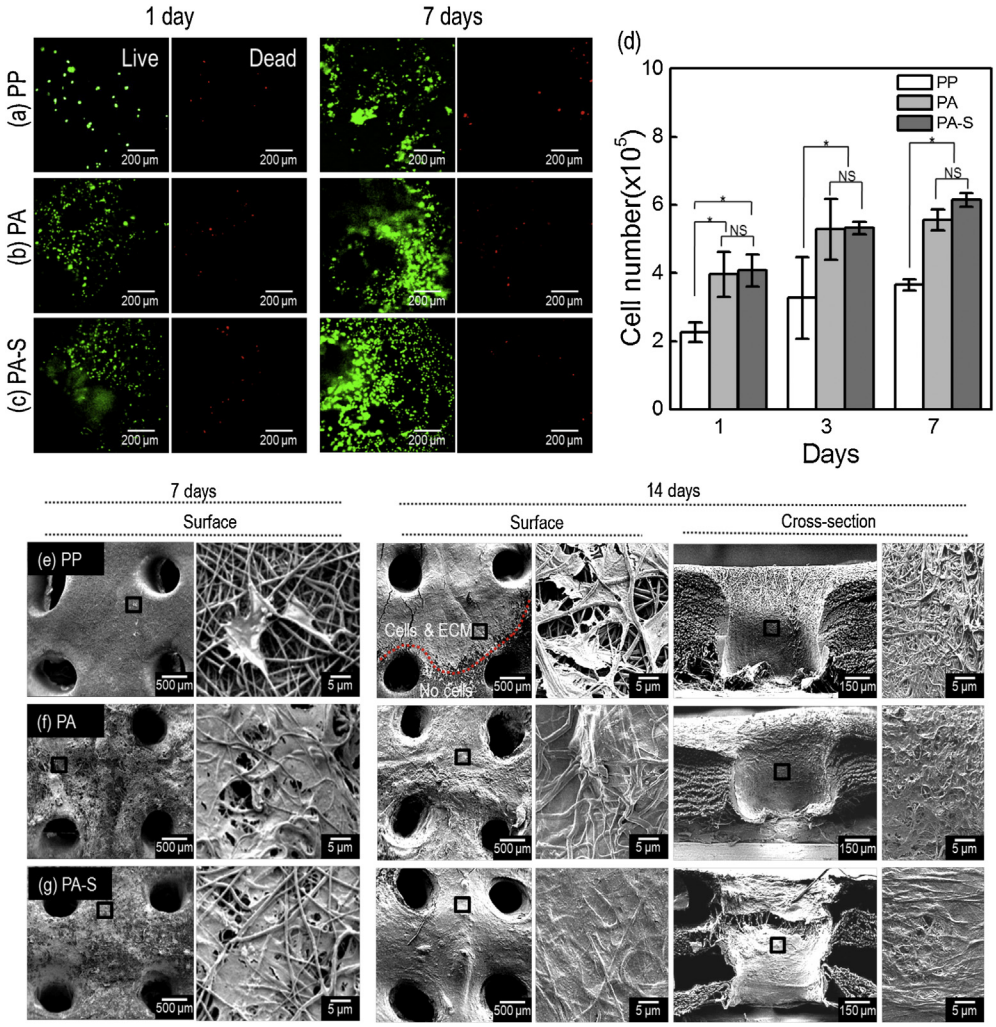

Fig. 5. Live (green) and dead (red) cell viability assay of (a) PP, (b) PA and (c) PA-S scaffolds after 1 and 7 days in culture. (d) Results of MTT assay after 1, 3 and 7 days of culture (PP, PA and PA-S). $^{*}P < 0.05$ indicates a significant difference and NS, a non-significant difference. Surface and cross-sectional SEM micrographs of MC3T3-E1 cells attached to (e) PP, (f) PA and (g) PA-S scaffolds after culture for 7 and 14 days.

Fig 5(d) shows the numbers of viable cells on the fibrous scaffolds at 1, 3 and 7 days of culture as determined by MTT assay. The cells proliferated on all fibrous scaffolds during the culture period. However, cell viability was significantly higher on the PA and PA-S scaffolds than the pure PCL scaffold (not significantly different between the PA and PA-S scaffolds). The MTT results were consistent with the live–dead analysis.

To assess the morphology of proliferated cells at 7 and 14 days, SEM images were obtained (Fig. 5(e–g)). As expected from the MTT results, at 7 days, the cells on the PA and PA-S scaffolds fully covered the surface, while proliferating cells were observed on the PP scaffold only sporadically. At 14 days, the cells fully covered both the surface and the cross-sectional area of the PA and PA-S scaffolds; however, for the PP scaffold, the cells did not completely cover the surface or cross-sectional area, indicated by the dotted line in Fig. 5(e).

These results were validated using fluorescence images showing the nuclei (blue) and F-actin (red) of cells on the surface of the scaffolds after 7 and 14 days of culture (Fig. 6(a–c)). The PA and PA-S fibrous scaffolds showed higher numbers of nuclei and a well-developed actin cytoskeleton versus the PP scaffold. This may be due to provision by the PCL/alginate scaffold of a more attractive microenvironment for the seeded cells, versus the pure PCL scaffold, even though the alginate was not modified with peptides, such as the RGD peptide.

3.5. Osteogenic expression

As typical markers of osteoblastic differentiation, ALP activity and calcium deposition were evaluated in the fibrous scaffolds. Both values were normalised to the total protein content (Table 3) for each culture day. Fig. 6(d) shows the ALP activity of MC3T3-E1 cells grown on the PP, PA and PA-S fibrous scaffolds for 7 and 14 days. At 7 days, ALP activity was not different between the scaffolds, but at 14 days a significant difference was evident. Additionally, the PA-S scaffolds showed the highest ALP levels after 14 days of culture. This may be due to the effect of mechanical properties on osteoblastic differentiation, because the cells can sense the mechanical stiffness of substrates through transmembrane molecules, such as integrins, and adjust their physiological processes through mechano-transduction (Ghosh & Ingber, 2007; Wang, Tytell, & Ingber, 2009).

Alizarin red S was used to visualise calcium mineralisation in the scaffolds. The optical density (OD) of alizarin red S extracted

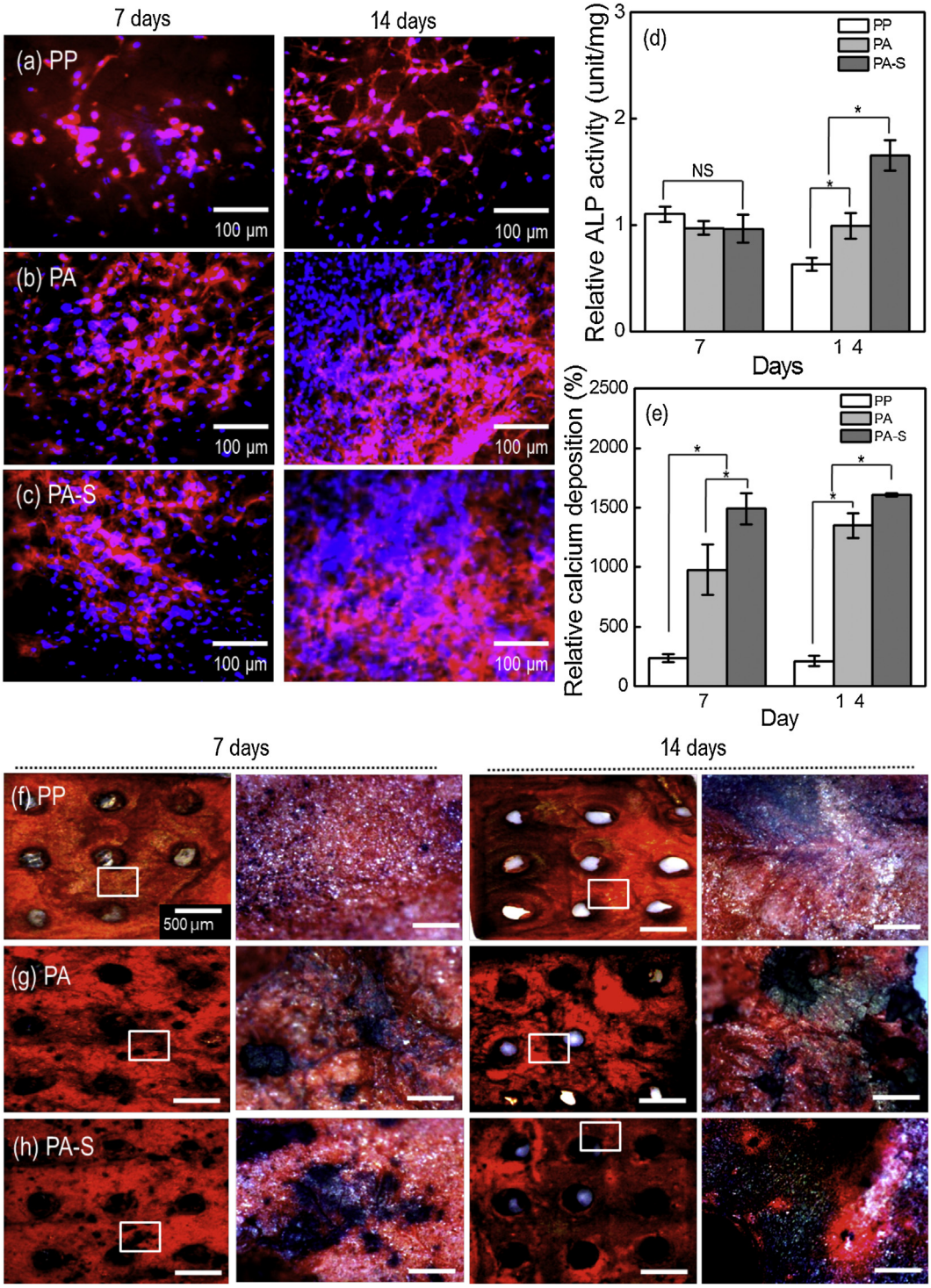

Fig. 6. Fluorescence surface and cross-sectional images of the (a) PP, (b) PA and (c) PA-S scaffolds after 7 and 14 days in culture. In this image, nuclei are stained blue and F-actin red. (d) Relative ALP activities and (e) calcium deposition levels of PP, PA and PA-S scaffolds. (f–h) Optical images of ARS staining of the scaffolds after 7 and 14 days of culture.

from stained scaffolds is shown in Fig. 6(e). Calcium deposition on the alginate-dispersed fibrous scaffolds (PA and PA-S) was considerably higher than on the PP scaffold, indicating that the alginate component provides more favourable micro-cellular environmental conditions, resulting in higher mineralisation versus the pure PCL scaffold. Fig. 6(f–h) show optical images of the alizarin red calcium assay at 14 days. A high intensity of alizarin red (black colouration) staining indicates a higher calcium concentration. The highest mineralisation was found in the PA-S scaffold.

Table 3
Total protein contents (mg) of PP, PA and PA-S scaffolds after culturing MG63 cells for 7 and 14 days.

	PP (mg)	PA (mg)	PA-S (mg)
7 days	69.15 ± 9.29	89.23 ± 12.78	91.50 ± 8.70
14 days	119.15 ± 24.75	120.97 ± 29.66	137.18 ± 10.87

4. Conclusions

In this study, PCL/alginate fibrous 3D scaffolds were fabricated by a combined method using wet electrospinning and rapid prototyping techniques. By accommodating an alginate component in the PCL/alginate composite scaffold, the hydrophilic and water absorption properties were greatly improved compared with the pure PCL scaffold, and the micro-sized PCL struts in the fibrous region provided the scaffold with greater mechanical properties compared with the pure fibrous scaffold. To demonstrate its feasibility as a hard-tissue regenerative material, *in vitro* cellular activities, including cell viability, proliferation and osteogenic differentiation (ALP activity and calcium mineralisation), were characterised using pre-osteoblast cells (MC3T3-E1). Although a small amount (5 wt%) of alginate, which was not modified with any peptides, was used, the PCL/alginate composite scaffolds (PAs) showed outstanding cell viability and proliferation. In particular, the PCL/alginate scaffold (PA-S) reinforced with PCL struts showed the highest level of osteogenic differentiation. Therefore, we suggest that this new PCL/alginate composite scaffold could be suitable for the regeneration of various hard tissues.

Acknowledgements

This study was supported by the National Research Foundation of Korea grant funded by the Ministry of Education, Science, and Technology (MEST) (Grant No. NRF-2012R1A2A2A01017435) .

References

Barnes, C. P., Sell, S. A., Boland, E. D., Simpson, D. G., & Bowlin, G. L. (2007). Nanofibre technology: Designing the next generation of tissue engineering scaffolds. *Advanced Drug Delivery Reviews*, *59*, 1413–1433.

Cohen, D. L., Malone, E., Lipson, H., & Bonassar, L. J. (2006). Direct freeform fabrication of seeded hydrogels in arbitrary geometries. *Tissue Engineering*, *12*, 1325–1335.

Discher, D. E., Janmey, P., & Wang, Y. (2005). Tissue cells feel and respond to the stiffness of their substrate. *Science*, *310*, 1139–1143.

Gallego, D., Ferrell, N., Sun, Y., & Hansford, D. J. (2008). Multilayer micromolding of degradable polymer tissue engineering scaffolds. *Materials Science and Engineering: C*, *28*, 353–358.

Galperin, A., Long, T. J., & Ratner, B. D. (2010). Degradable, thermo-sensitive poly(N-isopropyl acrylamide)-based scaffolds with controlled porosity for tissue engineering applications. *Biomacromolecules*, *11*, 2583–2592.

Ghosh, K., & Ingber, D. E. (2007). Micromechanical control of cell and tissue development: Implications for tissue engineering. *Advanced Drug Delivery Reviews*, *59*, 1306–1318.

Hollister, S. J. (2005). Porous scaffold design for tissue engineering. *Nature Materials*, *4*, 518–524.

Hong, S., & Kim, G. H. (2011). Fabrication of size-controlled three-dimensional structures consisting of electrohydrodynamically produced polycaprolactone micro/nanofibres. *Applied Physics A*, *103*, 1009–1014.

Hutmacher, D. W., & Biomater, J. (2001). Scaffold design and fabrication technologies for engineering tissues—State of the art and future perspectives. *Journal of Biomaterials Science Polymer Edition*, *12*, 107–124.

Karageorgiou, V., & Kaplan, D. (2005). Porosity of 3D biomaterial scaffolds and osteogenesis. *Biomaterials*, *26*, 5474–5491.

Kapyla, E., Aydogan, D. B., Virjula, S., Vanhatupa, S., Miettinen, S., Hyttinen, J., et al. (2012). Direct laser writing and geometrical analysis of scaffolds with designed pore architecture for three-dimensional cell culturing. *Journal of Micromechanics and Microengineering*, *22*, 115016.

Kim, M. S., Son, J. G., Lee, H. J., Hwang, H., Choi, C. H., & Kim, G. H. (2014). Highly porous 3D nanofibrous scaffolds processed with an electrospinning/laser process. *Current Applied Physics*, *14*, 1–7.

Kneser, U., Rath, S. N., Pryymachuk, G., Bleiziffer, O. A., Lam, C. X., Arkudas, A., et al. (2011). Hyaluronan-based heparin-incorporated hydrogels for generation of axially vascularised bioartificial bone tissues: *In vitro* and in vivo evaluation in a PLDLLA–TCP–PCL-composite system. *Journal of Materials Science: Materials in Medicine*, *22*, 1279–1291.

Koenig, M., & Huang, S. (1995). Biodegradable blends and composites of polycaprolactone and starch derivatives. *Polymer*, *36*, 1877–1882.

Kweon, H. Y., Yoo, M. K., Park, I. K., Kim, T. H., Lee, H. C., Lee, H. S., et al. (2003). A novel degradable polycaprolactone network for tissue engineering. *Biomaterials*, *24*, 801–808.

Langer, R., Vacanti, J. P., Vacanti, C. A., Atala, A., Freed, L. E., & Vunjak-Novakovic, G. (1995). Tissue engineering: Biomedical applications. *Tissue Engineering*, *1*, 151–161.

Lee, J., Jang, J., Oh, H., Jeong, Y. H., & Cho, D. W. (2013). Fabrication of a three-dimensional nanofibrous scaffold with lattice pores using direct-write electrospinning. *Materials Letters*, *93*, 397–400.

Liang, D., Hsiao, B. S., & Chu, B. (2007). Functional electrospun nanofibrous scaffolds for biomedical applications. *Advanced Drug Delivery Reviews*, *59*, 1392–1412.

Li, W.-J., Laurencin, C., Caterson, E., Tuan, R., & Ko, F. (2002). Electrospun nanofibrous structure: A novel scaffold for tissue engineering. *Journal of Biomedical Materials Research*, *60*, 613–621.

Ma, P. X. (2004). Scaffolds for tissue fabrication. *Materials Today*, *7*, 30–40.

Malafaya, P. B., Silva, G. A., & Reis, R. L. (2007). Natural-origin polymers as carriers and scaffolds for biomolecules and cell delivery in tissue engineering applications. *Advanced Drug Delivery Reviews*, *59*, 207–233.

Ma, Z., Kotaki, M., Inai, R., & Ramakrishna, S. (2005). Potential of nanofiber matrix as tissue engineering scaffolds. *Tissue Engineering*, *11*, 101–109.

Melchels, F. P. W., Barradas, A. M. C., van Blitterswijk, C. A., de Boer, J., Feijen, J., & Grijpma, D. W. (2010). Effects of the architecture of tissue engineering scaffolds on cell seeding and culturing. *Acta Biomaterialia*, *6*, 4208–4217.

Murphy, C. M., Haugh, M. G., & O'Brien, F. J. (2010). The effect of mean pore size on cell attachment, proliferation and migration in collagen–glycosaminoglycan scaffolds for bone tissue engineering. *Biomaterials*, *31*, 461–466.

Petrie Aronin, C. E., Cooper, J. A., Jr., Sefcik, L. S., Tholpady, S. S., Ogle, R. C., & Botchwey, E. A. (2008). Osteogenic differentiation of dura mater stem cells cultured *in vitro* on three-dimensional porous scaffolds of poly((-caprolactone) fabricated via co-extrusion and gas foaming. *Acta Biomaterialia*, *4*, 1187–1197.

Pham, Q. P., Sharma, U., & Mikos, A. G. (2006). Electrospinning of polymeric nanofibres for tissue engineering applications: A review. *Tissue Engineering*, *12*, 1197–1211.

Rezwan, K., Chen, Q. Z., Blaker, J. J., & Boccaccini, A. R. (2006). Biodegradable and bioactive porous polymer/inorganic composite scaffolds for bone tissue engineering. *Biomaterials*, *27*, 3413–3431.

Roosa, S. M., Kemppainen, J. M., Moffitt, E. N., Krebsbach, P. H., & Hollister, S. J. (2010). The pore size of polycaprolactone scaffolds has limited influence on bone regeneration in an *in vivo* model. *Journal of Biomedical Materials Research Part A*, *92*, 359–368.

Soliman, S., Sant, S., Nichol, J. W., Khabiry, M., Traversa, E., & Khademhosseini, A. (2011). Controlling the porosity of fibrous scaffolds by modulating the fibre diameter and packing density. *Journal of Biomedical Materials Research Part A*, *96A*, 566–574.

Vacanti, J. P., & Langer, R. (1999). Tissue engineering: The design and fabrication of living replacement devices for surgical reconstruction and transplantation. *Lancet*, *354*, S32–S34.

Vaquette, C., & Cooper-White, J. J. (2011). Increasing electrospun scaffold pore size with tailored collectors for improved cell penetration. *Acta Biomaterialia*, *7*, 2544–2557.

Wang, N., Tytell, J. D., & Ingber, D. E. (2009). Mechanotransduction at a distance: Mechanically coupling the extracellular matrix with the nucleus. *Nature Reviews Molecular Cell Biology*, *10*, 75–82.

Wu, H., Wan, Y., Dalai, S., & Zhang, R. (2010). Response of rat osteoblasts to polycaprolactone/chitosan blend porous scaffolds. *Journal of Biomedical Materials Research Part A*, *92*, 238–245.

Yang, S., Leong, K. F., Du, Z., & Chua, C. K. (2001). The design of scaffolds for use in tissue engineering. Part I. Traditional factors. *Tissue Engineering*, *7*, 679–689.

Zhou, Y., Hutmacher, D. W., Varawan, S. L., & Lim, T. M. (2007). *In vitro* bone engineering based on polycaprolactone and polycaprolactone–tricalcium phosphate composites. *Polymer International*, *56*, 333–342.

Zhu, Y., Gao, C., Liu, X., & Shen, J. (2002). Surface modification of polycaprolactone membrane via aminolysis and biomacromolecule immobilisation for promoting cytocompatibility of human endothelial cells. *Biomacromolecules*, *3*, 1312–1319.